ELSEVIER

NeuroImage

www.elsevier.com/locate/ynimg
NeuroImage 33 (2006) 570–579

Bayesian estimation of cerebral perfusion using a physiological model of microvasculature

Kim Mouridsen,[a,*] Karl Friston,[b] Niels Hjort,[a] Louise Gyldensted,[a] Leif Østergaard,[a] and Stefan Kiebel[b]

[a]*Department of Neuroradiology, Centre of Functionally Integrative Neuroscience, Building 30, Århus University Hospital, Nørrebrogade 44, DK-8000 Århus C, Denmark*
[b]*Wellcome Department of Imaging Neuroscience, Institute of Neurology, London, UK*

Received 14 February 2006; revised 7 June 2006; accepted 18 June 2006

Perfusion weighted MRI has proven very useful for deriving hemodynamic parameters such as CBF, CBV and MTT. These quantities are important diagnostically, e.g. in acute stroke, where they are used to delineate ischemic regions. Yet the standard method for estimating CBF based on singular value decomposition (SVD) has been demonstrated to underestimate (especially high) flow components and to be sensitive to delays in the arterial input function (AIF). Furthermore, the estimated residue functions often oscillate. This compromises their physiological interpretation/basis and makes estimation of related measures such as flow heterogeneity difficult. In this study, we estimate perfusion parameters based on a vascular model (VM) which represents heterogeneous capillary flow and explicitly leads to monotonically decreasing residue functions. We use a fully Bayesian approach to obtain posterior probability distributions for all parameters. In simulation studies, we show that the VM method has less bias in CBF estimates than the SVD based method for realistic SNRs. This also applies to cases where the AIF is delayed. We employ our method to estimate perfusion maps using data from (i) a healthy volunteer and (ii) from a stroke patient.

Keywords: Cerebral blood flow (CBF); Dynamic susceptibility contrast MRI; Vascular model; Bayesian analysis; Deconvolution; Singular value decomposition (SVD)

Introduction

Dynamic susceptibility contrast magnetic resonance imaging (DSC-MRI) is widely used for quantification of cerebral perfusion. Several studies have shown that perfusion parameters such as cerebral blood flow (CBF) and mean transit time (MTT) can be used in acute stroke patients for delineating the 'penumbra'; defined here as tissue with normal diffusion characteristics but abnormal perfusion, believed to be at risk of infarct, yet salvageable (Baird and Warach, 1998; Sorensen et al., 1999). A key issue in inferring crucial physiological information from perfusion imaging is the conversion of the observed concentration time curve (CTC) into reliable estimates of CBF, CBV and MTT. Assuming the injected bolus is an impulse MTT can be estimated by integrating the normalized CTC, but since this assumption does not hold, even for rapid i.v. injection of contrast agent, most techniques are based on the tracer kinetic observation that the observed CTC is the convolution of the AIF with a residue function, scaled by CBF. The residue function represents the fraction of observed tracer remaining in the observed vasculature at a certain time after its arrival. The predominate techniques for estimating CBF are based on deconvolving the AIF with the CTC using singular value decomposition (SVD) to estimate the impulse response (defined as the residue function multiplied by CBF). Its maximum value is CBF (Ostergaard et al., 1996; Wu et al., 2003).

Whereas CBF estimates are crucial in delineating critically hypoperfused tissue and in obtaining accurate MTT values, the shape of the residue function reflects microvascular retention of tracer and thereby the distribution of capillary velocities (Ostergaard et al., 1999). Indeed, it has been speculated that changes in capillary perfusion patterns may reflect regulatory mechanisms of significance in severe ischemia (Ostergaard et al., 2000; Perkio et al., 2005; Simonsen et al., 2002). Therefore, high accuracy in estimating CBF *and* the residue function is of key importance for the study and diagnosis of acute stroke.

Concentration curves obtained using DSC-MRI typically exhibit a relatively high noise level (low SNR). This has been demonstrated

Abbreviations: AIF, arterial input function; CBF, cerebral blood flow; CBV, cerebral blood volume; CTC, concentration time curve; DSC, dynamic susceptibility; EM, expectation maximization; EPI, echo planar imaging; MCA, middle cerebral artery; MTT, mean transit time; SNR, signal to noise ratio; SPM, statistical parametric mapping; SVD, singular value decomposition; oSVD, circular SVD; sSVD, standard SVD (same as SVD); VM, vascular model.

* Corresponding author.
E-mail address: kimm@pet.auh.dk (K. Mouridsen).
Available online on ScienceDirect (www.sciencedirect.com).

1053-8119/$ - see front matter © 2006 Elsevier Inc. All rights reserved.
doi:10.1016/j.neuroimage.2006.06.015

to cause underestimation of CBF especially for low SNR (Ostergaard et al., 1996). Generally, deconvolution is an ill-posed problem where small changes in the data (the concentration time curve) may dramatically influence the response (residue function). Consequently, any deconvolution technique will produce residue functions which are intrinsically rough and irregular, lacking the smoothness and monotonic properties of physiologically admissible solutions (the fraction of contrast agent as a function of time, after an impulse injection, is a decreasing function of time).

More robust deconvolution techniques are primarily obtained through regularization of the residue function. In so-called Gaussian Process deconvolution (Andersen et al., 2002), it is suggested that Gaussian priors are used for individual time points of the residue function. This produces a smoother estimate of the residue function. The method was shown to compare well to SVD for high SNRs and results in less biased estimates for low SNRs. A smooth estimate of the residue function can also be obtained using Tikhonov regularization where an oscillation penalty is applied in a least squares solution (Calamante et al., 2003).

Another problem encountered in DSC-MRI analysis is the estimation of delay between the measured AIF and the observed concentration time curve. It has been demonstrated that the standard SVD underestimates CBF when the AIF lags the concentration time curve (Calamante et al., 2002; Ostergaard et al., 1996). However, an extended version of SVD known as circular SVD (oSVD) has been shown to be insensitive to tracer arrival times (Wu et al., 2003).

In this work, we present a novel estimation procedure that resolves all these problems by using an appropriate forward or generative model of the signal. This is based on a physiological model for the capillaries. By modeling the dynamics of the microvasculature, we ensure smooth, monotonically decreasing estimates of the residue function. Furthermore, in contrast to SVD methods, our residue function estimate is completely characterized by only two parameters. These can be used to assess efficiently how the shape of the residue function varies among brain regions. Our approach also has the advantage of allowing prior information about model parameters to be incorporated into the analysis. For estimation, we use a Bayesian system identification approach (Friston et al., 2003) based on an EM-algorithm, implemented in the functional imaging analysis package Statistical Parametric Mapping (SPM) (http://www.fil.ion.ucl.ac.uk/spm/).

Following a description of the theoretical framework of the vascular model and the estimation procedure, we present a simulation study, which shows that our procedure compares well to the SVD methods for low flows but does not underestimate high flows and is unaffected by low SNR. Furthermore, we demonstrate that the algorithm is robust to delays between the AIF and the CTC. The procedure is then applied to perfusion data from a normal healthy subject and compared to the performance of standard SVD (sSVD) and oSVD. To illustrate the practical use of the present approach, we use the algorithm to obtain CBF estimates in a patient with middle cerebral artery (MCA) occlusion. On these data, we also assess anecdotally the performance of the vascular model relative to sSVD and oSVD in ischemic tissue.

Theory

We assume for a given tissue voxel that the intravascular tracer is delivered to the capillaries from an arteriole and denote by $C_a(t)$ the tracer concentration at time t in the feeding arteriole. According to indicator-dilution theory, the concentration of tracer in the capillaries at time t is proportional to the convolution of $C_a(t)$ with the residue function $R(t)$

$$\kappa C(t) = \mathrm{CBF}\int_0^t C_a(\tau)R(t-\tau)d\tau \tag{1}$$

The residue function describes the fraction of tracer still present in the capillaries at time t. The constant κ depends on the hematocrit levels in the arteriole and capillaries and the density of brain tissue. Since these parameters are generally indeterminable, κ is usually replaced by an arbitrary but fixed value (Calamante et al., 1999; Kennan and Jäger, 2003). If we can estimate the product $\mathrm{CBF}\cdot R(t)$ we obtain an estimate for CBF because $R(0)=1$. Using this estimate, we can calculate MTT using the central volume theorem (Stewart, 1894)

$$\mathrm{MTT} = \frac{\mathrm{CBV}}{\mathrm{CBF}} \tag{2}$$

where

$$\mathrm{CBV} = \frac{\int C(t)\mathrm{d}t}{\int C_a(t)\mathrm{d}t}.$$

Often, these conventional estimates are complemented by some delay estimation. The delay is defined as the time it takes for the arterial blood to arrive at the voxel of interest. This delay can be estimated as the time point corresponding to the maximum of $\mathrm{CBF}\cdot R(t)$.

When $C(t)$ and $C_a(t)$ have been measured at M time points, the convolution in Eq. (1) (with $\kappa=1$) can be written as

$$\mathrm{C}(t_i) = \mathrm{CBF}\cdot\Delta t\cdot\sum_{j=1}^{i} C_a(t_j)R(t_i-t_j) \tag{3}$$

Eq. (3) can also be written in matrix notation as

$$\mathrm{CBF}\cdot\Delta t\cdot\mathbf{A}\mathbf{r} = \mathbf{c} \tag{4}$$

where

$$\mathbf{A} = \begin{pmatrix} C_a(t_1) & 0 & \cdots & 0 \\ C_a(t_2) & C_a(t_1) & & 0 \\ \vdots & & \ddots & \\ C_a(t_M) & C_a(t_{M-1}) & & C_a(t_1) \end{pmatrix} \text{ and } \mathbf{r} = \begin{pmatrix} R(t_1) \\ R(t_2) \\ \vdots \\ R(t_M) \end{pmatrix}.$$

The critical step in this procedure is the estimation of the residue function. One non-parametric method for this is based on singular value decomposition (SVD). The matrix $\mathbf{A}$ can be written as

$$\mathbf{A} = \mathbf{U}\mathbf{L}\mathbf{V}^{\mathrm{T}}$$

where the columns of $\mathbf{U}$ are the eigenvectors of $\mathbf{A}\mathbf{A}^{\mathrm{T}}$ and $\mathbf{L}$ is a diagonal matrix of the corresponding eigenvalues (Mardia et al., 1979). Since all matrices on the right hand side in this equation may be inverted, we can obtain an expression for the inverse of $\mathbf{A}$ and hence solve for $\mathbf{r}$ in Eq. (4)

$$\mathrm{CBF}\cdot\Delta t\cdot\mathbf{r} = \mathbf{V}\mathbf{L}^{-1}\mathbf{U}^{\mathrm{T}}\mathbf{c}$$

In order to regularize the solution for $\mathbf{r}$, elements in $\mathbf{L}$ below a certain threshold are set to zero. This threshold is usually set to 20% of the maximum element in $\mathbf{L}$ (Ostergaard et al., 1996).

Vascular model

A key issue is how to find a parametric representation of the residue function which is informed by a physiological model of microvasculature. We consider a vascular dynamic model similar to (Kroll et al., 1996; Ostergaard et al., 1999) (see Fig. 1). We model the capillary system as N parallel tubes where the transit time for a particle entering tube i is T_i. When blood is delivered to the capillaries from the feeding artery, it is distributed among these tubes and the fraction entering the i'th tube is denoted as h_i. Hence, the h_i's comprise a discretized approximation (determined by the values of T_i) to the density function of the transit times (Fig. 1). Since the arterial input function is not necessarily measured close to the tissue voxel, we let the parameter δ model the delay encountered between the artery and the capillaries.

The ensuing residue function is given by

$$\mathrm{R}_i = \sum_{j>i} h_j = 1 - \sum_{j \le i} h_j.$$

By setting $R(t_i)=1-\sum_{i\le t_i} h_j$ in Eq. (3) the parameters $h=(h_1, \ldots, h_N)$ can, in principle, be estimated by fitting the right hand side of Eq. (3) to an observed concentration time curve.

However, the number of tubes needed for a good approximation to the continuous model Eq. (1) may be rather large. This makes this parameterization impractical for estimation because the number of parameters is proportional to the number of tubes. Furthermore, the particular transit times would have to encompass different tissue types under normal as well as pathological conditions. A high number of tubes with similar transit times will lead to imprecise estimates. A simple way of reducing the effective number of parameters is to assume a parametric form $h(t;\theta)$ of the transport function $h(t)$, where θ is a vector of model parameters. Experience with kinetic models of this sort suggests that the family of gamma distributions

$$\mathrm{h}(t;\alpha,\beta) = \frac{1}{\beta^{\alpha}\Gamma(\alpha)} t^{\alpha-1} e^{-t/\beta}, \qquad \alpha,\beta > 0$$

with shape parameter $\alpha>0$ and scale parameter $\beta>0$ is sufficiently flexible. Note that when $\alpha=1$ this is an exponential distribution with mean β; when $\alpha=f/2$ and $\beta=1$ this is a chi-squared distribution with f degrees of freedom (see also Fig. 3). In the following, we will let $\alpha=\lambda$ and $\beta=\mathrm{CBV}/(\lambda\cdot\mathrm{CBF})$ to ensure that the mean transit time, which is the product of α and β, is equal to CBV/CBF in accordance with Eq. (2). We will demonstrate in the simulations that our parameterization captures all the important features of the transit function. The residue function is now given by

$$R(t) = \int_{\mathrm{t}}^{\infty} h(\tau;\alpha,\beta)\mathrm{d}\tau$$

which can be inserted into Eq. (1). For any set of model parameters, this enables us to evaluate a predicted concentration time curve $C(t)$ which can be evaluated numerically (cf. Eq. (3)).

To avoid errors due to undersampling, and to estimate delays, which are not integer multiples of the TR, we fit a cubic spline to the measured AIF and resample it at eight times the TR. The free parameters of the vascular model are $\theta=(\mathrm{CBF}, \lambda, \delta)$ and in the following we describe how these can be estimated, based on Eq. (3).

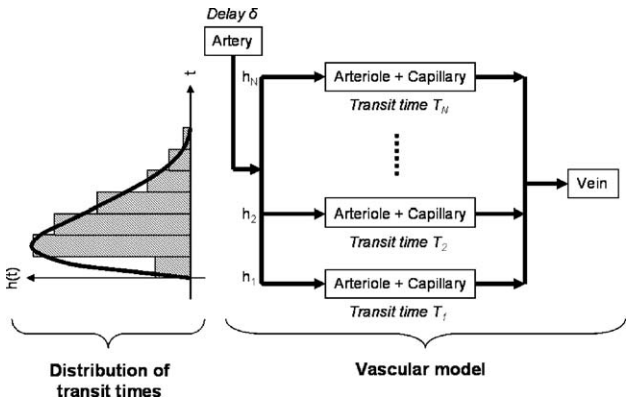

Fig. 1. Schematic representation of the vascular model. Blood is delivered to the tissue with a delay δ relative to the measured arterial input function. Within the tissue, particles are distributed to a number of tubes (N), each with different transit time T_i. The fraction of particles distributed to tube i is h_i. The h_i's form an empirical density function for the transit times which characterizes the microvasculature. This is indicated by the histogram on the left hand side. By increasing the number of tubes, the histogram will converge to and represent an estimate of the underlying continuous density function $h(t)$ for the transit times t.

Observation model

When the paramagnetic contrast agent passes through the capillaries, the transverse relaxation rate R_2 changes linearly in proportion to the intravascular concentration C of the agent

$$R_2 = R_2^0 + r_2 C$$

where R_2^0 is the intrinsic SE relaxation rate without the contrast and r_2 is the transverse relaxivity (Villringer et al., 1988; Weisskoff et al., 1994). Assuming a mono-exponential relaxation the signal intensity for a T_2-weighted sequence is $S=S_0\exp(-TE\cdot R_2)$, where TE is the echo time and S_0 is a constant depending on proton density, repetition time and longitudinal relaxation time, T_1. Hence, the concentration of intravascular contrast agent $C(t)$ at time t in a tissue voxel is related to the MR signal by

$$\begin{aligned} C(t) &= r_2^{-1}(R_2(t) - R(0)) \\ &= -\frac{1}{r_2 TE}\log\left(\frac{S(t)}{S(0)}\right) \end{aligned} \qquad (5)$$

where $S(0)$ is the baseline signal measured before bolus arrival. We can therefore think of the model described above as a single-input single output (SISO) system where the input is the arterial input function $C_a(t)$ and the response is the concentration $C(t)$ which is measured indirectly through the output non-linearity $S(t)=S(0)e^{-r_2C(t)TE}$. Fig. 2 combines the system and output equations to show the form of our forward or likelihood model.

We assume that the signal can be decomposed into a deterministic component $s(t)$ plus a noise component $\varepsilon(t)$ such that $S(t)=s(t)+\varepsilon(t)$ where $\varepsilon(t)\sim N(0,\sum_\varepsilon)$. This means that the likelihood function $L(S|\sum_\varepsilon)$ is a multidimensional Gaussian pdf. Theoretically, the MR signal is not Gaussian since it is the magnitude of a complex signal (and can not be negative), leading to a so-called Rician distribution (Sijbers et al., 1998). However, this distribution is approximately normal when the SNR is high (Gudbjartsson and

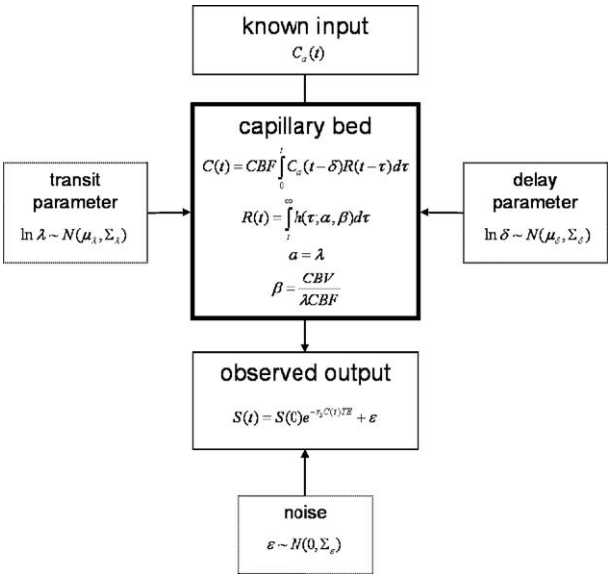

Fig. 2. Illustration of the non-linear observation model. This is a single input-single output system where the input is the arterial input function $C_a(t)$, and the measured output is the signal intensity curve $S(t)$. We assume that the measured signal can be decomposed into a true signal $S_{True}(t)$ and a zero-mean Gaussian error term. The measured signal is determined by the unobserved concentration time curve which is the response of the capillary network. This is fully determined by the parameters α,β of the transport function h.

Patz, 1995; Sijbers et al., 1998). Note, however, that normality is not guaranteed after the non-linear transformation to concentration time curves, Eq (5), which is the reason we choose to directly model the MR signal intensity $S(t)$ in this study.

Bayesian modeling

A common problem with pure frequentist models is their inability to incorporate prior knowledge about model parameters. This information may range from simple interval constraints to detailed knowledge of distributional properties revealed in previous or related studies. Increased flexibility in model building can be achieved using a Bayesian framework. In Bayesian modeling, knowledge about the parameters of interest is embodied in the form of a prior distribution on the parameters. In our case, we need to ensure that all parameters are positive. Therefore, we let the prior distribution be log-normal, i.e. $\log\theta$ has a Gaussian distribution.

The posterior distribution of θ is then given by Bayes' rule

$$p(\theta|S) = \frac{p(\theta)L(S|\theta)}{\int_\Theta p(\theta)L(S|\theta)\mathrm{d}\theta}.$$

Note that if the log-transformed parameters are used, then the prior as well as the likelihood is Gaussian and therefore the product of the two is again Gaussian (Gelman et al., 2003). In order to obtain the posterior mean and covariance matrix of θ, we apply a Bayesian system identification approach first described in Friston et al. (2003). This is based on a Levenberg–Marquart type Expectation–Maximization (EM) algorithm. This procedure is implemented in SPM5 (Statistical Parametric Mapping www.fil.ion.ucl.ac.uk/spm/software/spm5) and has already been used extensively for fMRI and EEG data (Friston et al., 2003; Kiebel et al., 2006). The output of the Bayesian analysis is the posterior multivariate distribution of the parameters. This allows us to make inferences using the posterior expectation and covariances of the parameters.

The Bayesian framework has one further advantage over frequentist statistics. One can compute the model evidence, which is useful for model selection (Penny et al., 2004). Although we forgo any model comparisons in the present paper, we note that model selection is useful for comparing alternative, competing models for the same data.

Prior distributions

It is possible to add no further information to the model than the positivity constraint by setting the diagonal elements of the covariance matrix (the parameter variances) to infinity. But it is more natural to use readily available approximations to CBF and MTT to specify the mean of the prior distribution. Here we use the area of the concentration time curve normalized by the area of the AIF as the prior CBV and we use the SVD to provide the prior mean of CBF. Then using the central volume theorem we obtain an estimate of MTT. The prior mean of the delay parameter is set to the time point when the SVD residue function attains its maximum. The covariance matrix for the parameter vector was a diagonal matrix with fixed values for the prior variances (see Materials and methods).

Materials and methods

Simulations

An AIF was simulated using a gamma-variate function which has been used previously for the parameterization of input functions (Rausch et al., 2000). The AIF $C_a(t)$ has the following analytic expression

$$C_a(t) = \begin{cases} 0 & t \le t_0 \\ a(t-t_0)^b e^{-(t-t_0)/c} & t > t_0 \end{cases}$$

where we set $a=1$, $t_0=0$, $b=3$ and $c=1.5$ to render an input function with a shape and size that would typically be obtained using a standard injection scheme (Calamante et al., 2000; Ostergaard et al., 1996). Simulations were performed for CBV=4% and 2% which is considered representative of normal gray and white matter (Leenders et al., 1990). Flow values were varied from 10 to 70 ml/100g/min in 10 ml/100 g/min increments for CBV=4% and from 5 to 35 ml/100 g/min in 5 ml/100 g/min increments for CBV=2%. In this way, we obtain the same MTT range in each case, 3.43 s to 24 s, where MTT is calculated using the central volume theorem Eq. (2). We used the shape parameter λ to generate two different types of residue functions. By setting $\lambda=1$, we get exponential residue functions and setting $\lambda=100$ we get residue functions which are approximately box-car functions, see Fig. 3. Concentration time curves were generated as described in Vascular model using Eq. (3).

Signal curves $S(t)$ were generated using $S(t)=S_0\exp(-\kappa C(t)\mathrm{TE})$ with $S_0=100$ and TE=65 ms. The constant κ was chosen such that a flow of 60 ml/100g/min and blood volume 4% produces a 40% signal drop relative to the baseline S_0 as is typical for normal gray matter (Calamante et al., 2000; Ostergaard et al., 1996). The signal curve for the AIF was generated similarly but with κ calibrated to give a peak signal drop of 60%. Zero mean Gaussian noise was added to the signal curves to produce baseline SNRs of either 20 or 100. These values cover the noise range typically found in our

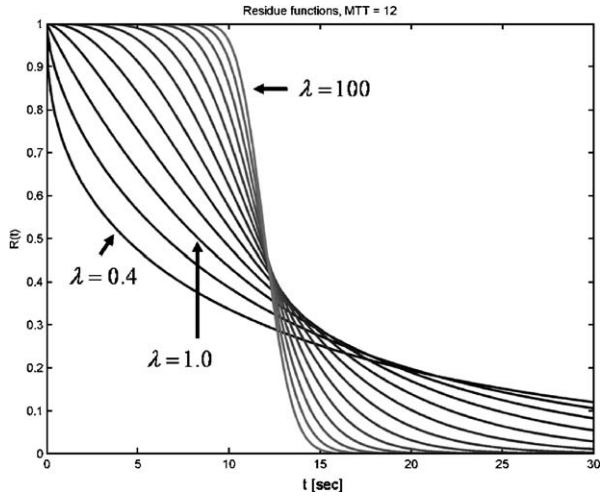

Fig. 3. Examples of residue functions with identical MTT (12 s) but different values of the shape parameter λ. When $\lambda=1$, the residue function is exponential and with increasing λ, $R(t)$ converges to a box-car function.

clinical data, and have been used in previous studies on deconvolution methodology (Wu et al., 2003). Finally, the signal curves were transformed back to concentration time curves. For each combination of CBV and CBF, a total of 100 concentration time curves were generated.

To analyze the case where there is a substantial delay between the AIF and the concentration time curve, the AIF curve was shifted up to 5 units, in one unit increments, each time generating another 100 sample concentration time curves for each CBV, CBF combination.

Estimates of CBF were obtained using the vascular model (VM), standard SVD (sSVD) and circular SVD (oSVD). The prior means for CBF and delay δ were specified as described in 'Bayesian modeling'. No ad hoc estimate of the shape parameter λ is available and therefore the prior mean was fixed at $\lambda_0=10$. The prior covariance of $\log\theta=\log(\mathrm{CBF}, \lambda, \delta)$ was a diagonal matrix with elements (0.1, 10, 10). The prior variances of λ and δ were higher than the prior variance of flow since these parameters may realistically come close to zero. This corresponds to large negative values on the log-scale, far away from the prior mean. In general, the prior covariance matrix depends on the quality of the data and the prior means. For sSVD, we used a threshold of 20% as suggested in Ostergaard et al. (1996). In the case of oSVD, we fixed the oscillation index at 0.065 when SNR = 100 and 0.035 for SNR = 20 as in Wu et al. (2003).

Empirical data acquisition

One 64 year old healthy male volunteer was scanned with axial Spin Echo EPI (TR/TE = 1499/75 ms) on a 1.5 T GE Signa LX imager (GE Medical Systems, Milawukee, WI) during I.V bolus injection (5 ml/s) of 0.2 mmol/kg gadobutrol (Gadovist® 1.0 M, Schering) immediately followed by 20 ml saline. One slice, matrix 128 × 128, at the level of the middle cerebral artery (M1) was analyzed.

To study the performance of our algorithm in ischemic tissue, we analyzed perfusion data from a 63 year old female with a right-sided MCA occlusion, scanned 5 h after symptom onset on a 3.0 T GE Signa imager (GE Medical Systems, Milawukee, WI) during I.V bolus injection (5 ml/s) of 0.1 mmol/kg gadobutrol (Gadovist® 1.0 M, Schering) and gradient echo, EPI (TR/TE 1500/45 ms). A contralateral AIF was determined automatically using a cluster analysis algorithm (Mouridsen et al., 2006). The SVD threshold was fixed at 20% and the oSVD threshold set to 0.095 (Ostergaard et al., 1996; Wu et al., 2003). The prior mean and covariance of parameters in the vascular model were identical to those applied in the simulation study. A follow up T2 scan was performed after 3 months.

Results

Simulations

Examples of typical residue functions obtained using VM, sSVD and oSVD are shown in Fig. 4 for SNR = 100 and 20. In both cases, the true flow is 20 ml/100 g/min and the true residue function is a box-car function. For SNR = 100, the shape of VM residue function is in excellent agreement with the true residue function while the curve estimated using sSVD oscillates moderately around the true

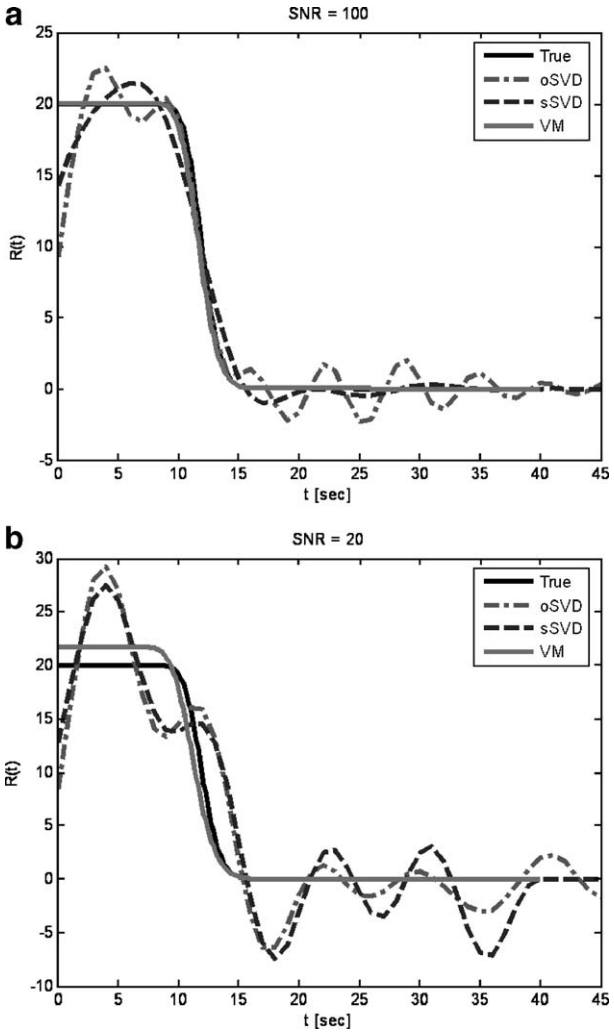

Fig. 4. Typical residue functions obtained with the vascular model, sSVD and oSVD (CBF = 20 ml/100g/min, CBV = 4%, $\lambda=100$, zero delay). For SNR = 100 (top) and SNR = 20 (bottom), the VM estimates of $R(t)$ are in close agreement with the true residue function. In comparison, the sSVD and particularly the oSVD estimates exhibit large oscillations and periodically take negative values when the true $R(t)$ is zero.

curve. In comparison, the oSVD residue function exhibits large oscillations and takes negative values on some intervals When SNR = 20, the oscillations in both the sSVD and oSVD residue functions are even more pronounced. For experiment times when the true residue function is close to zero, both SVD estimates alternate between positive and negative values. The residue function obtained with the VM is in good agreement with the true curve.

The ability to correctly estimate true CBF in the range 10 to 70 ml/100g/min when CBV = 4% is summarized in Fig. 5 for the VM, sSVD and oSVD. When SNR = 100, the VM produces flow estimates in excellent agreement with the true values uniformly in the flow spectrum whereas the SVD methods seem unable to reproduce high flow components. When a delay of 5 times TR is introduced between the AIF and the concentration time curve, the VM flow estimates are only marginally biased in the high end of the range, while the sSVD estimates have dropped further compared to the case without delay. In line with previous findings (Wu et al., 2003), we note that oSVD estimates of CBF are close to the estimates obtained when there is no delay. Also in the case of box-car residue functions, the VM flow estimates are unbiased. Interestingly,

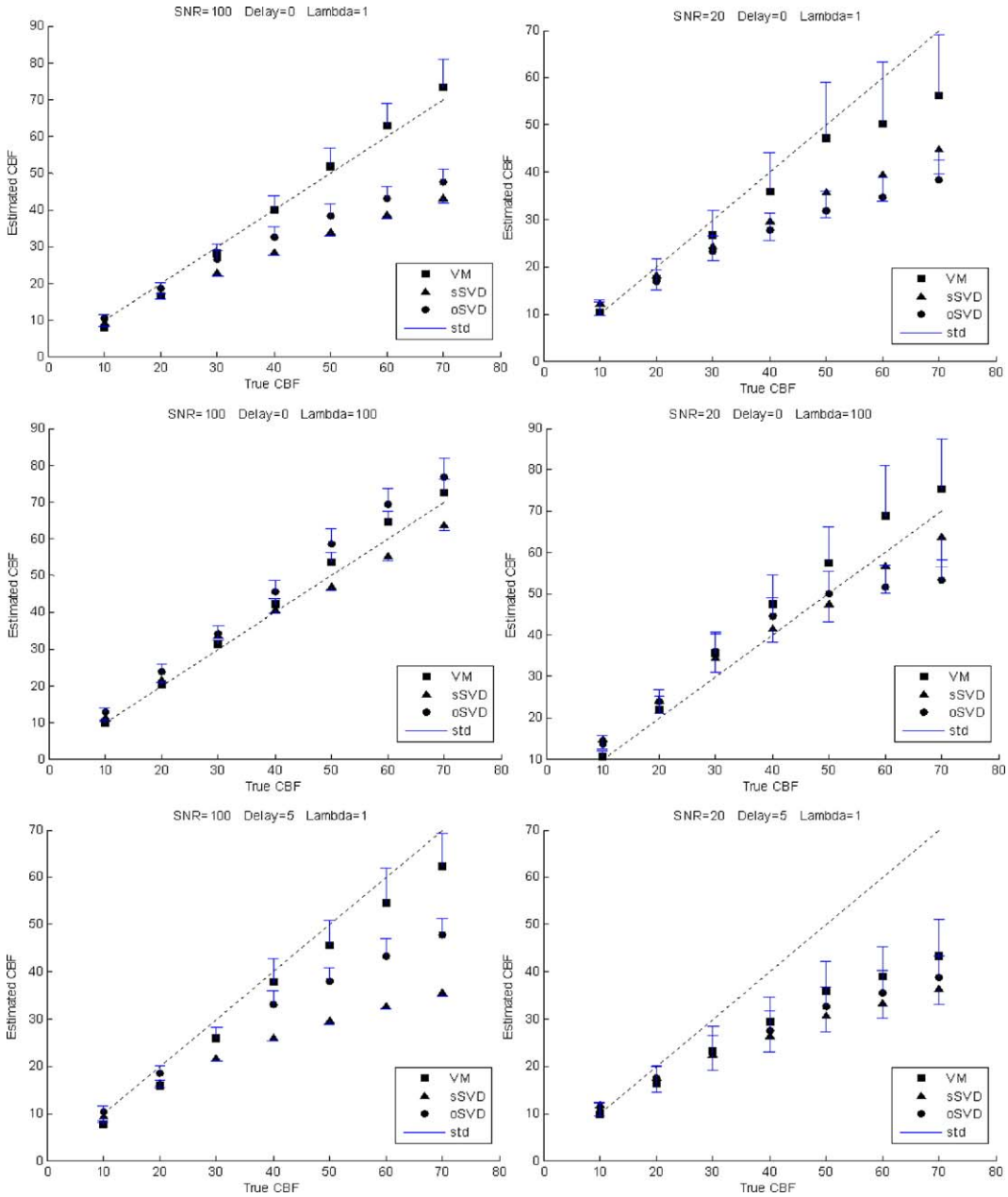

Fig. 5. Illustration of the association between true or simulated and estimated flow (in ml/100 g/min) in the Monte Carlo simulations for the VM and o/sSVD (CBV = 4%). When SNR = 100 (left column), the bias in VM flow estimates is small compared to o/sSVD estimates. The sSVD estimates demonstrate the smallest standard deviations around their means but the bias depends on both delay and underlying residue function. In contrast, oSVD estimates have a higher standard deviation but depends only on $R(t)$. The same relations between VM and SVD estimates are observed when SNR = 20 (right column) except for an increased bias in VM estimates and a general increase in standard deviations.

the bias in both SVD methods is negligible compared to exponential residue functions.

When SNR = 20, all estimates generally exhibit larger bias and higher standard errors. For exponential residue functions, the flow estimates derived using the VM are closer to the true values compared to the SVD methods. This is also true in the case of delay between the AIF and the CTC, although here the VM starts to show a curvi-linear relation between simulated and estimated values comparable to the SVD methods. For box-car residue functions, the bias in VM flow estimates is higher than in the case where SNR = 100, but the relation is still linear, which is not the case for oSVD estimates.

In Fig. 5, deviations from true flows are seen in the high end of the flow range, while deviations of the same relative size for low flows are much harder to detect. Therefore, we used the ratio between the estimated and the true flow as a measure of agreement that is independent of the size of the true flow. To compare the three algorithms, we calculated the mean and standard deviation of this ratio for each of the algorithms under all simulation conditions. The results are shown in Tables 1 and 2 for CBV equal to 4% and 2%, respectively. The values in Table 1 correspond to the plots in Fig. 5. Table 2 shows that when CBV = 2%, the VM has a mean CBFest/CBFtrue ratio closest to unity, compared to the SVD methods when the residue function is exponential (0.93 ± 0.16 (VM) compared to 0.74 ± 0.11 (sSVD) and 0.83 ± 0.16 (oSVD) when SNR = 100, and 0.95 ± 0.35 (VM) compared to 0.90 ± 0.36 (sSVD) and 0.75 ± 0.27 (oSVD) when SNR = 20).

Clinically acquired human MRI data

In order to compare the performance of the vascular model on actual perfusion data, to sSVD and oSVD, we calculated CBF, MTT and delay maps using each of these methods, respectively. Results are shown in Fig. 6. CBF and MTT maps were standardized by normalization to white matter. For the CBF images, the grey/white matter contrast is good when using VM and in addition the high flows in the anterior vessels (the MCA branches) are well reproduced using this approach relative to the SVD methods. This is consistent with the simulations. Note also that the dynamic range of VM estimates is larger than for SVD, which we speculate may lead to improved delineation of ischemic penumbra. Furthermore, the VM correctly estimates very long mean transit times in the ventricles which the contrast agent does not enter if the blood–brain barrier is intact. The ventricles are less clearly delineated on the SVD MTT maps.

We analyzed the acute PWI data from a 63 year old female presenting with occlusion of the MCA. The resulting CBF, MTT and delay maps are shown in Fig. 7. CBF and MTT images are standardized by normalization to white matter. In particular, the VM, but also sSVD, estimates lower flows in the posterior MCA territory compared to oSVD. MTT maps show a clear distinction between ischemic and normally perfused tissue. However, the dynamic range of the MTT values estimated using the VM is large compared to the SVD maps and the contrast to non-ischemic tissue is particularly clear in this case. No systematic differences between methods are observed on the delay maps except that quantitatively oSVD estimates are higher than VM and sSVD estimates.

Discussion

We have presented a general statistical framework for estimation of perfusion parameters based on a parametric model for the microvasculature. The major motivation is the observation that direct unconstrained fitting of Eq. (1) to an observed concentration time curve leads to oscillating residue functions, which have no physiological interpretation. These instabilities in the estimates are due to the ill-posedness of the inverse problem. Although the oscillations may be reduced by adding a roughness penalty in the optimization procedure, monotonicity is not guaranteed and the influence on CBF estimates is unclear.

The key idea in our work is to consider a model for the microvasculature and assume a parametric form of the transport function that defines the distribution of transit times in the capillaries. We used the gamma-variate pdf because the corresponding family of residue functions encompasses a wide range of shapes which are representative of normal ($R(t)$ exponential) as well as ischemic tissue ($R(t)$ box-car). However, experimental data to guide selection of an appropriate parametric family are scarce. Other models could be used as well (e.g., Lorenzians). Furthermore, in cases of low SNR, the exact functional form of $R(t)$ might not be critical for estimating perfusion. We note that a principled approach to explore alternative parameterizations is model comparison using Bayes factors (Penny et al., 2004).

Assuming a parametric form of the residue function, only the key quantities flow, delay and residue function shape parameters need to be estimated, whereas in non-parametric approaches every point on the residue function must be estimated. Note that the residue function is guaranteed to be monotonically decreasing without introducing separate regularization. Although the choice of a vascular model potentially limits the generality of this approach, a main finding of this study is that the Bayesian approach and the flexibility of the model allows the flow estimation for a variety of residue functions, at least as accurately as with SVD methods.

Essentially, the task of estimating the model parameters for a given concentration time curve is a non-linear regression problem. As such any algorithm such as Gauss–Newton for solving non-linear least squares optimization problems can be used. However, the ill-posedness of the problem in practical situations calls for prior information to reduce bias and variance in parameter estimates. Therefore, we propose a Bayesian estimation scheme.

Table 1
Mean ratios between estimated and true CBF values in the Monte Carlo simulations (mean ± standard deviation)

	SNR = 100			SNR = 20		
	VM	SVD	oSVD	VM	SVD	oSVD
Exponential	0.95 ± 0.13	0.73 ± 0.10	0.83 ± 0.14	0.90 ± 0.22	0.82 ± 0.23	0.73 ± 0.20
Exponential, delay = 5	0.87 ± 0.11	0.68 ± 0.14	0.83 ± 0.14	0.75 ± 0.20	0.73 ± 0.24	0.74 ± 0.20
Box-car	1.04 ± 0.05	1.01 ± 0.09	1.16 ± 0.10	1.13 ± 0.18	1.10 ± 0.24	1.07 ± 0.24

CBV = 4%.

Table 2
Mean ratios between estimated and true CBF values in the Monte Carlo simulations (mean±standard deviation)

	SNR=100			SNR=20		
	VM	SVD	oSVD	VM	SVD	oSVD
Exponential	0.93±0.16	0.74±0.12	0.82±0.17	0.98±0.39	0.93±0.41	0.74±0.27
Exponential, delay=5	0.81±0.11	0.68±0.16	0.82±0.17	0.85±0.40	0.85±0.43	0.76±0.30
Box-car	1.07±0.09	1.02±0.11	1.18±0.14	1.28±0.36	1.20±0.40	1.06±0.33

CBV=2%.

We have evaluated the performance of the algorithm using Monte Carlo simulations. Our results indicate that for an SNR of 100 the estimated flow values exhibit negligible bias throughout a flow range of 10–70 ml/100 g/min under exponential as well as box-car flow distributions. Furthermore, the estimated flow values were independent of delay. This signifies an improved ability to discriminate flow components compared to the SVD methods. When the signal to noise ratio is low (SNR=20), the mismatch is increased for high delay and when the residue function is box-car. This behavior is most likely due to the low SNR, because the SVD-based methods show similar or larger mismatches. However, with the present method, we can employ more informative priors (see below) and still compute meaningful results when SNR is low.

The simulations confirm previous findings that sSVD is sensitive to delay whereas oSVD estimates are unaffected by temporal shifts of the AIF. Both methods exhibit a non-linear relation between true and estimated flow where notably high flow components are poorly reproduced. Interestingly, this non-linearity is negligible for box-car residue functions. Our anecdotal results on the performance of the VM in clinical MR data suggest that the present approach can correctly reproduce high flows and establish a degree of face validity, see Fig. 6. Moreover, the ischemic region in the stroke patient with MCA occlusion seems more clearly outlined on the MTT map, relative to the SVD-based maps (Fig. 7). However, we are aware that this claim can only be substantiated by further experiments and evaluations of multiple patients' data. The clinical data are included to illustrate the application of the present method to real data. We hope that these analyses demonstrate the potential of the technique.

It should be noted, that although delay can be modeled using this parametric approach, our technique does not accommodate dispersion effects. This is because it is difficult to separate reliably

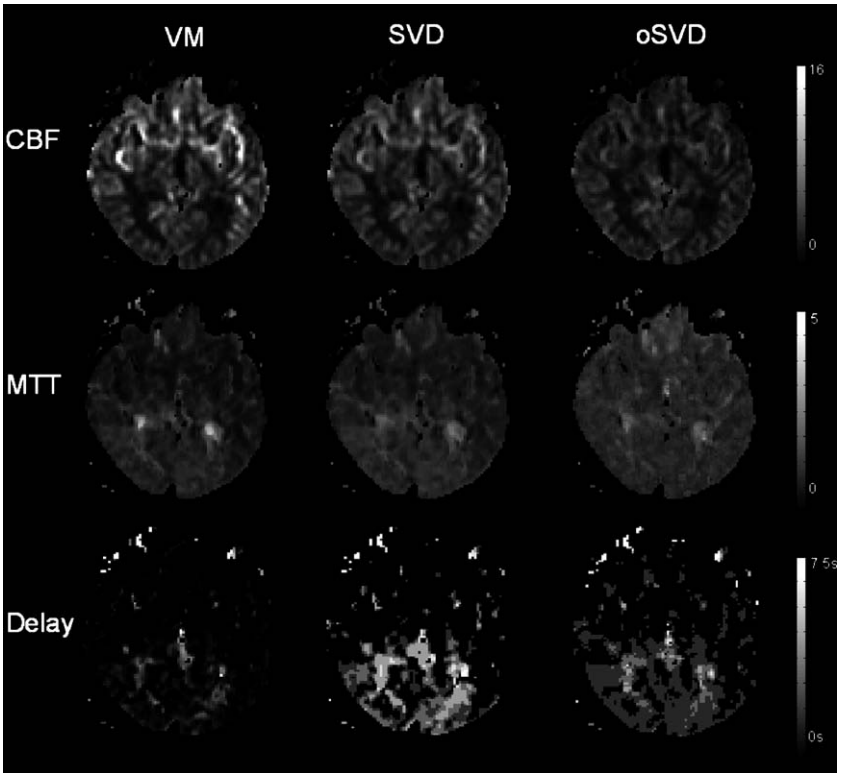

Fig. 6. Perfusion maps estimated using the VM, o/sSVD. CBF and MTT values are standardized to white matter (the VM CBF map and oSVD delay maps have been slightly cropped due to a few outliers). The ability of the VM to correctly reproduce high flow components is signified in the CBF map where the MCA branches are clearly delineated. Moreover there seems to be a marked contrast between grey and white matter. Relative VM and sSVD CBF estimates are on the same scale while the dynamical range in the oSVD map was smaller. There is some discrepancy between delay maps. The VM estimates delay to be lower than o/sSVD estimates.

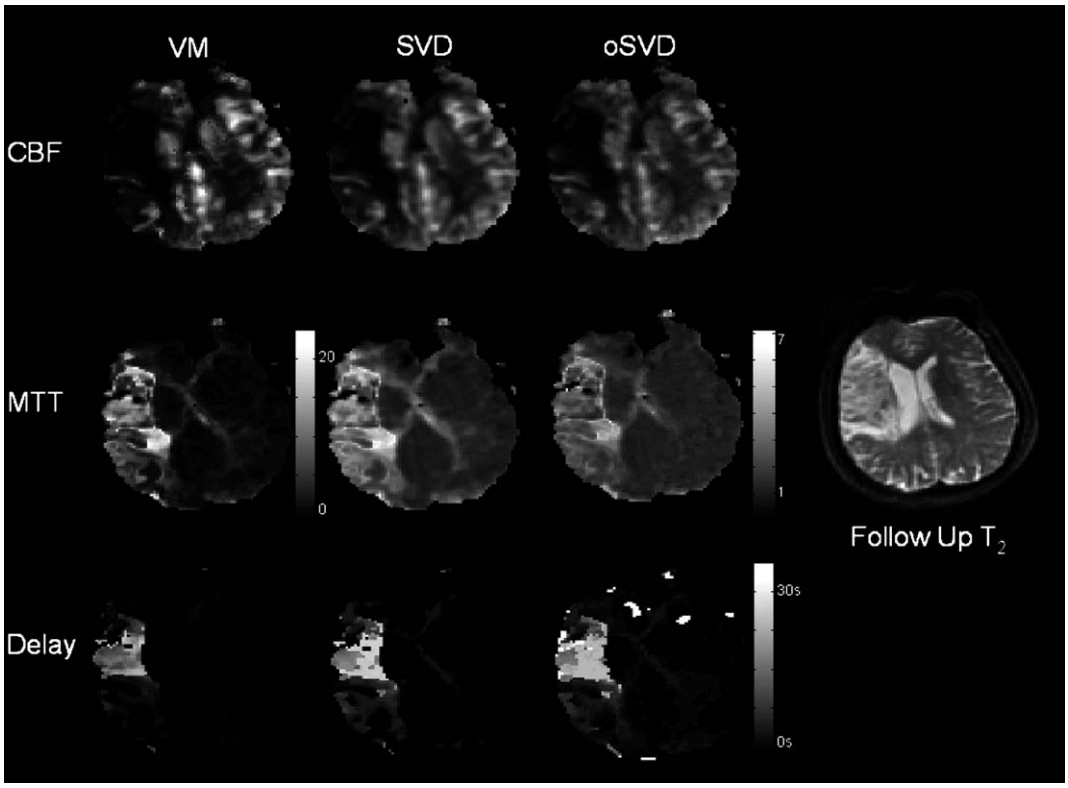

Fig. 7. Perfusion maps obtained with VM and o/sSVD for patient with acute MCA occlusion. CBF and MTT values are relative to normal appearing white matter (the VM CBF map and oSVD delay map have been slightly cropped due to a few outliers). The 3 month follow-up T2 is shown to the right. There is a clear contrast between vessels, grey/white matter and the ischemic region in the VM CBF map. However, all methods seem to overestimate the posterior extent of the final infarct.

microvascular retention from retention in the feeding vessels due to the strong correlation of the relevant parameters. In theory, a voxel-specific AIF can be estimated by convolving the measured $C_a(t)$ with a function describing transport from the site of AIF measurement to the voxel in question. This estimate will depend on the global vascular architecture and is therefore not adequate in pathology. However, both delay and dispersion effects may be minimized by using local arterial input functions as described in (Alsop et al., 2002) or (Calamante et al., 2004).

An additional benefit of our model is that the residue function is characterized using only two parameters representing shape and scale (or dispersion). We speculate that these parameters can be used to produce maps representing capillary flow profiles and that such maps may further help assess the tissue viability in ischemia. In particular, the smooth residue functions estimated using the VM may lead to improved estimation of flow heterogeneity (Ostergaard et al., 1999, 2000), which is determined using the first derivative of $R(t)$. This in turn results in a better characterization of microscopic flow profiles. As an initial approach, these parameters may be entered into predictive algorithms (Wu et al., 2001) together with traditional perfusion and diffusion indices to quantify the relative predictive value of these parameters.

The ability to include prior information is a key feature in the model. Although it is possible to employ uninformative priors, we have used an empirical Bayes approach for which we obtained prior means as simple functions of the data. These should be seen as initial 'ballpark' estimates. A similar informative prior would let the prior mean and covariance depend on CBV, measured SNR and/or classified tissue type. However, to obtain useful prior information from clinical data, we need to extract this information from a large age-matched control group. With such a spatially normalized data base, it would be rather straightforward to obtain tissue- or even voxel-specific priors.

Acknowledgments

The authors wish to thank Søren Christensen for many interesting discussions. This study was supported by the Danish National Research Foundation, the Danish Medical Research Council, Schering AG, GlaxoSmithKline, The Wellcome Trust and Carl and Ellen Hertz' Grant.

References

Alsop, D.D., Wedmid, A., Schlaug, G., 2002. Defining a local input function for perfusion quantification with bolus constrast MRI. Proc. ISMRM.

Andersen, I.K., Szymkowiak, A., Rasmussen, C.E., Hanson, L.G., Marstrand, J.R., Larsson, H.B.W., Hansen, L.K., 2002. Perfusion quantification using Gaussian process deconvolution. Magn. Reson. Med. 48, 351–361.

Baird, A.E., Warach, S., 1998. Magnetic resonance imaging of acute stroke. J. Cereb. Blood Flow Metab. 18, 583–609.

Calamante, F., Thomas, D.L., Pell, G.S., Wiersma, J., Turner, R., 1999. Measuring cerebral blood flow using magnetic resonance imaging techniques. J. Cereb. Blood Flow Metab. 19, 701–735.

Calamante, F., Gadian, D.G., Connelly, A., 2000. Delay and dispersion

effects in dynamic susceptibility contrast MRI: simulations using singular value decomposition. Magn. Reson. Med. 44, 466–473.

Calamante, F., Gadian, D.G., Connelly, A., 2002. Quantification of perfusion using bolus tracking magnetic resonance imaging in stroke: assumptions, limitations, and potential implications for clinical use. Stroke 33, 1146–1151.

Calamante, F., Gadian, D.G., Connelly, A., 2003. Quantification of bolus-tracking MRI: improved characterization of the tissue residue function using Tikhonov regularization. Magn. Reson. Med. 50, 1237–1247.

Calamante, F., Morup, M., Hansen, L.K., 2004. Defining a local arterial input function for perfusion MRI using independent component analysis. Magn. Reson. Med. 52, 789–797.

Friston, K.J., Harrison, L., Penny, W., 2003. Dynamic causal modelling. NeuroImage 19, 1273–1302.

Gelman, A., Carlin, J., Stern, H., Rubin, D., 2003. Bayesian Data Analysis, 2nd ed. Chapman and Hall/CRC.

Gudbjartsson, H., Patz, S., 1995. The Rician distribution of noisy MRI data. Magn. Reson. Med. 34, 910–914.

Kennan, R., Jäger, H.R., 2003. T2- and T2*-w DCE-MRI: blood perfusion and volume estimation using bolus tracking. In: Tofts, P. (Ed.), Quantitative MRI of the Brain. John Wiley and Sons, Ltd.

Kiebel, S.J., David, O., Friston, K.J., 2006. Dynamic Causal Modelling of Evoked Responses in EEG/MEG with lead-field parameterization. NeuroImage 30 (4), 1273–1284.

Kroll, K., Wilke, N., Jerosch-Herold, M., Wang, Y., Zhang, Y., Bache, R.J., Bassingthwaighte, J.B., 1996. Modeling regional myocardial flows from residue functions of an intravascular indicator. Am. J. Physiol.: Heart Circ. Physiol. 40, H1643–H1655.

Leenders, K.L., Perani, D., Lammertsma, A.A., Heather, J.D., Buckingham, P., Healy, M.J.R., Gibbs, J.M., Wise, R.J.S., Hatazawa, J., Herold, S., Beaney, R.P., Brooks, D.J., Spinks, T., Rhodes, C., Frackowiak, R.S.J., Jones, T., 1990. Cerebral blood-flow, blood-volume and oxygen utilization-normal values and effect of age. Brain 113, 27–47.

Mardia, K.V., Kent, J.T., Bibby, J.M., 1979. Multivariate Analysis. Academic Press, London.

Mouridsen, K., Christensen, S., Gyldensted, L., Østergaard, L., 2006. Automatic selection of arterial input function using cluster analysis. Magn. Reson. Med. 55 (3), 524–531.

Ostergaard, L., Weisskoff, R.M., Chesler, D.A., Gyldensted, C., Rosen, B.R., 1996. High resolution measurement of cerebral blood flow using intravascular tracer bolus passages: 1. Mathematical approach and statistical analysis. Magn. Reson. Med. 36, 715–725.

Ostergaard, L., Chesler, D.A., Weisskoff, R.M., Sorensen, A.G., Rosen, B.R., 1999. Modeling cerebral blood flow and flow heterogeneity from magnetic resonance residue data. J. Cereb. Blood Flow Metab. 19, 690–699.

Ostergaard, L., Sorensen, A.G., Chesler, D.A., Weisskoff, R.M., Koroshetz, W.J., Wu, O., Gyldensted, C., Rosen, B.R., 2000. Combined diffusion-weighted and perfusion-weighted flow heterogeneity magnetic resonance imaging in acute stroke. Stroke 31, 1097–1103.

Penny, W.D., Stephan, K.E., Mechelli, A., Friston, K.J., 2004. Comparing dynamic causal models. NeuroImage 22, 1157–1172.

Perkio, J., Soinne, L., Ostergaard, L., Helenius, J., Kangasmaki, A., Martinkauppi, S., Salonen, O., Savolainen, S., Kaste, M., Tatlisumak, T., Aronen, H.J., 2005. Abnormal intravoxel cerebral blood flow heterogeneity in human ischemic stroke determined by dynamic susceptibility contrast magnetic resonance imaging. Stroke 36, 44–49.

Rausch, M., Scheffler, K., Rudin, M., Radu, E.W., 2000. Analysis of input functions from different arterial branches with gamma variate functions and cluster analysis for quantitative blood volume measurements. Magn. Reson. Imaging 18, 1235–1243.

Sijbers, J., den Dekker, A.J., Van Audekerke, J., Verhoye, M., Van Dyck, D., 1998. Estimation of the noise in magnitude MR images. Magn. Reson. Imaging 16, 87–90.

Simonsen, C.Z., Rohl, L., Vestergaard-Poulsen, P., Gyldensted, C., Andersen, G., Ostergaard, L., 2002. Final infarct size after acute stroke: prediction with flow heterogeneity. Radiology 225, 269–275.

Sorensen, A.G., Copen, W.A., Ostergaard, L., Buonanno, F.S., Gonzalez, R.G., Rordorf, G., Rosen, B.R., Schwamm, L.H., Weisskoff, R.M., Koroshetz, W.J., 1999. Hyperacute stroke: simultaneous measurement of relative cerebral blood volume, relative cerebral blood flow, and mean tissue transit time. Radiology 210, 519–527.

Stewart, G.N., 1894. Researches on the circulation time in organs and on the influences which affect it: Parts I–III. J. Physiol. 15.

Villringer, A., Rosen, B.R., Belliveau, J.W., Ackerman, J.L., Lauffer, R. B., Buxton, R.B., Chao, Y.S., Wedeen, V.J., Brady, T.J., 1988. Dynamic imaging with lanthanide chelates in normal brain-contrast due to magnetic-susceptibility effects. Magn. Reson. Med. 6, 164–174.

Weisskoff, R.M., Zuo, C.S., Boxerman, J.L., Rosen, B.R., 1994. Microscopic susceptibility variation and transverse relaxation—Theory and experiment. Magn. Reson. Med. 31, 601–610.

Wu, O., Koroshetz, W.J., Ostergaard, L., Buonanno, F.S., Copen, W.A., Gonzalez, R.G., Rordorf, G., Rosen, B.R., Schwamm, L.H., Weisskoff, R.M., Sorensen, A.G., 2001. Predicting tissue outcome in acute human cerebral ischemia using combined diffusion- and perfusion-weighted MR imaging. Stroke 32, 933–942.

Wu, O., Ostergaard, L., Weisskoff, R.M., Benner, T., Rosen, B.R., Sorensen, A.G., 2003. Tracer arrival timing-insensitive technique for estimating flow in MR perfusion-weighted imaging using singular value decomposition with a block-circulant deconvolution matrix. Magn. Reson. Med. 50, 164–174.